Electromagnetic Tracking Using Modular, Tiled Field Generators

Herman Alexander Jaeger, *Member, IEEE*, and Pádraig Cantillon-Murphy, *Senior Member, IEEE*

***Abstract*— Electromagnetic tracking (EMT) systems play an important role in medicine, robotics, and virtual reality applications by providing accurate position and orientation referencing within a fixed volume around a magnetic field generator. Advances in sensor technology provide increasingly small, lightweight sensors capable of being integrated into hand-held devices for medical simulation, gaming, and image-guided surgery. The need for customizable tracking volumes becomes of interest as the uptake of EMT technology increases. This paper proposes a new method of creating custom tracking volumes from multiple planar field generators. A monolithic, low-cost printed circuit board design allows for *tiling* of multiple generators to create a larger tracking volume. Experiments were performed with two generators at different angles. Successful tracking is demonstrated with increased positional accuracy observed when transmitters are inclined with respect to one another. Horizontal tiling configurations are most accurate when a common edge is shared between adjacent field generators.**

***Index Terms*— Biot–Savart law, electromagnetic tracking (EMT), image-guided therapy, magnetic tracking, modular generator, planar magnetics, surgical navigation, virtual reality.**

I. Introduction

ELECTROMAGNETIC tracking (EMT) systems are becoming an increasingly common position and orientation reference tool. Short-range tracking applications include virtual reality [1] and surgical navigation applications [2], while long-range tracking applications include pedestrian tracking [3] and drill navigation [4]. Tracking is performed using a magnetic sensor, which detects the local magnetic field in order to resolve its absolute position and orientation relative to the origin of the magnetic field source. The term EM refers to the use of EM induction to produce a spatially unique time-varying magnetic field in which an induction coil sensor may be tracked [5]. This paper focuses on small tracking volumes for the precise tracking and navigation of medical devices such as ultrasound [6] and airway navigation [7]. Advances in coil winding technology allow for fabrication of tracking sensors of submillimeter dimensions [8], facilitating integration within small robotic manipulators and minimally invasive medical devices [9], [10].

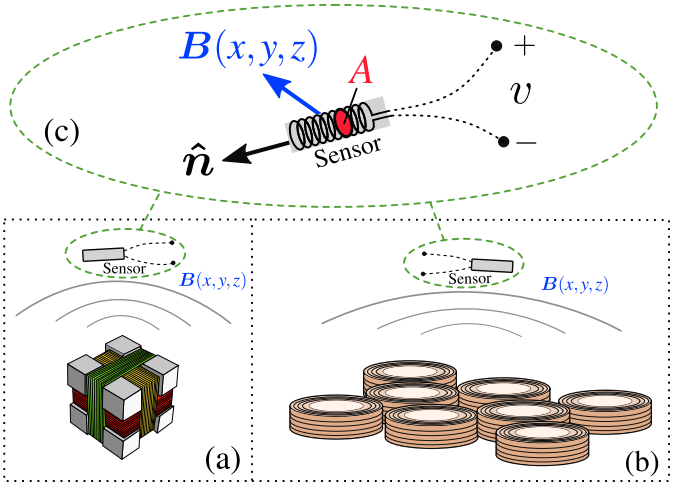

Fig. 1. (a) Illustration of a triaxial field generator consisting of three orthogonal windings on a cube former. (b) Illustration of a planar field generator design consisting of multiple circular coils. (c) Magnetic sensor detects the component of the generated magnetic flux density $\boldsymbol{B}$ that is aligned axially with the sensor's cross-sectional area A with normal vector $\hat{\boldsymbol{n}}$.

EMT systems invariably share two common components: a magnetic field generator and a magnetic receiver. The generator establishes a low-frequency time-varying magnetic field such that each point in the vicinity of the generator has a unique magnetic signature dependent on the distance from the generator. Many field generator topologies exist and feature different magnetic field designs. Triaxial generator designs as shown in Fig. 1(a) [1], [11] are by far the most common as they provide a sufficiently unique magnetic field distribution using three orthogonal coils. Generators that use multiple planar coils as shown in Fig. 1(b) [12], [13] are also common, which enables the generator to be planar in shape allowing tracking over large areas, though this form factor requires a higher coil count to achieve a spatially unique magnetic field. In general, for a solenoidal tracking sensor receiver shown in Fig. 1(c), the induced voltage signal v is proportional to the magnetic flux density $\boldsymbol{B}$ produced by the generator at the point (x, y, z) projected along the axis $\hat{\boldsymbol{n}}$ of the sensor. Recent work has shown that even a single uniaxial transmitter can be used to successfully achieve six degree-of-freedom tracking, although this requires a relatively advanced sensor design capable of sensing both dc and ac magnetic signals [14].

Manuscript received October 22, 2018; revised January 7, 2019; accepted February 9, 2019. This work was supported in part by the Science Foundation Ireland Technology Innovation and Development under Award TIDA17/4897 and in part by the Eureka Eurostars Project under Grant 11581 entitled Mariana: Image-guided catheter navigation in the outer airways. The Associate Editor coordinating the review process was Daniele Fontanelli. *(Corresponding author: Herman Alexander Jaeger.)*

H. A. Jaeger is with the School of Engineering, University College Cork, T12 K8AF Cork, Ireland (e-mail: h.jaeger@umail.ucc.ie).

P. Cantillon-Murphy is with the School of Engineering, Tyndall National Institute, University College Cork, T12 R5CP Cork, Ireland (e-mail: p.cantillonmurphy@ucc.ie).

Color versions of one or more of the figures in this paper are available online at http:ieeexplore.ieee.org.

Digital Object Identifier 10.1109/TIM.2019.2900884

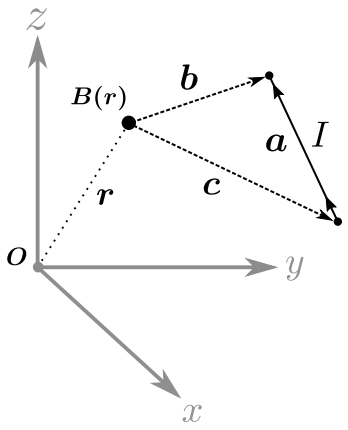

Fig. 2. Vectors in (2).

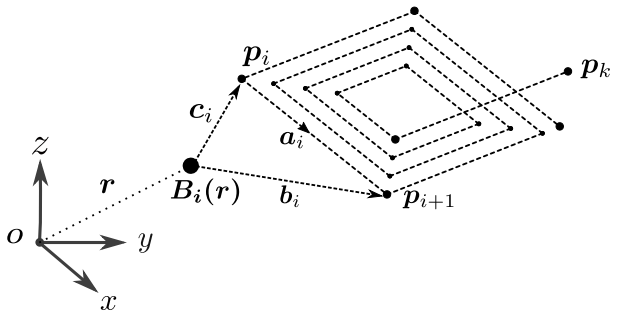

Fig. 3. Current filament model illustrated for multiple straight line segments of a single PCB coil. The total magnetic field of the coil $\boldsymbol{B}_{\text{coil}}$ at the position $\boldsymbol{r}$ is the superposition of all fields caused by each line segment $\boldsymbol{a}_i$ (4).

As the applications of EMT continue to expand, the requirement for modular tracking volumes becomes of particular interest. At present, the only commercially available systems that readily support expandable tracking volumes are the Liberty Latus and G4 tracking systems (Polhemus Inc, Colchester, VT, USA) in which multiple field generators can work in tandem to form an aggregate tracking volume; however, their modular tracking methods are proprietary. No readily scalable field generator design has been reported in the literature at the time of writing. Previous work that can offer scalability include the tracking system designs of [3] and [5], although in both cases, errors in the order of centimeters are reported, which make them unsuitable for precision applications. An increasingly accurate discrete field generator coil array was described in [15] to enable the wireless tracking of tumors during radiotherapy with reported errors of less than 2 mm, although the large size of the field generator limits its potential uses in other medical applications.

This paper describes a novel method of constructing a customized magnetic tracking volume using multiple planar printed circuit board (PCB) field generators. The previously reported EMT platform [16] is demonstrated with a configurable tracking volume using two such generators. The magnetic field model for the system is developed and experiments are performed for various field generator configurations. Though only two field generators were used in experimental work, the method can be readily scaled for N field generators in order to provide customized position and orientation referencing in volumes defined by the research application.

II. Planar EM Tracking

The tracking system used in this paper utilizes a planar magnetic field generator implemented in a PCB and is capable of tracking a five degree-of-freedom (DoF) solenoidal coil sensor in a 25 cm × 25 cm × 25 cm volume [10]. The induced voltage signals on the sensor are numerically fit to an analytical magnetic model of the field generator to yield the position and orientation of the sensor. This information can be represented as 5-DoF vector in the following:

$$\boldsymbol{r} = [x, y, z, \theta, \varphi]^T . \tag{1}$$

A combination of trust-region and Levenburg–Marquardt algorithms [17], [18] is used for the solving process. Complete details regarding the algorithm can be found in [19]. The coils that emit the magnetic signal are constructed using predefined copper traces in a planar array [13]. Advantages of this design include high precision and repeatability in the coil design due to the manufacturing process.

A. Magnetic Field Model

The tracking system uses a current filament approach to model the generator's magnetic field [19]. The coils are square and constructed from multiple straight-line copper traces with a pitch of 0.75 mm on a monolithic two-layer PCB with a thickness of 1.6 mm. The magnetic field due to each line trace of a coil is derived from the Biot–Savart law in [20] and is given by

$$\boldsymbol{B}(\boldsymbol{r}) = \frac{\mu_0 I}{4\pi}\left(\frac{\boldsymbol{c}\times\boldsymbol{a}}{|\boldsymbol{c}\times\boldsymbol{a}|^2}\right)\left(\frac{\boldsymbol{a}\cdot\boldsymbol{c}}{|\boldsymbol{c}|} - \frac{\boldsymbol{a}\cdot\boldsymbol{b}}{|\boldsymbol{b}|}\right) \tag{2}$$

where $\boldsymbol{B}$ is a vector signifying the magnetic flux density in Tesla, $\boldsymbol{a}$ is a vector representing the length and the direction of a current carrying conductive filament. The vector $\boldsymbol{r}$ points from the origin, $\boldsymbol{O}$, to the observation point from which the field due to the filament is measured. Vectors $\boldsymbol{c}$ and $\boldsymbol{b}$ point from the observer position $\boldsymbol{r}$ to the start and end points of the current filament, respectively, and I is the filament current in amperes and μ_0 is the magnetic permeability of free space. Fig. 2 shows a graphical representation of (2) for a single copper trace element. The resultant magnetic flux density vector $\boldsymbol{B}$ is given by

$$\boldsymbol{B} = \left[B_x, B_y, B_z\right]^T \tag{3}$$

where B_x, B_y, and B_z are the Cartesian flux density components referenced to the origin, $\boldsymbol{O}$.

The tracking system field generator coils consist of multiple filament elements as illustrated in Fig. 3, where each filament is defined by a pair of points, $[\boldsymbol{p}_i, \boldsymbol{p}_{i+1}]$, in Cartesian coordinates with respect to the origin. The total magnetic field due to all filaments of a coil at some position $\boldsymbol{r}$ can then be calculated by summing all the individual filament field

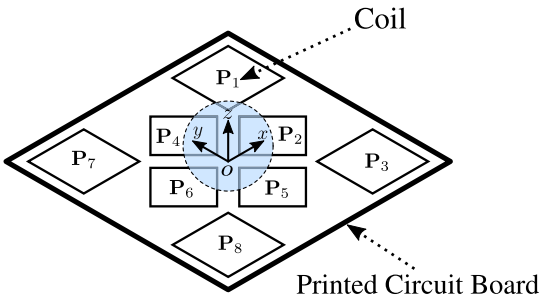

Fig. 4. Location of each transmitter coil relative to the origin, $\boldsymbol{O}$, for a field generator circuit board containing $M = 8$ coils.

contributions, given by

$$\boldsymbol{B}_{coil} = \sum_{i=1}^{k-1} \boldsymbol{B}_i(\boldsymbol{r}) \tag{4}$$

where $k-1$ is the total number of filaments comprising a coil defined by k points.

Now, consider a field generator comprising of multiple coils as shown in Fig. 4, where coil filaments are defined with respect to the geometric center of the coil arrangement. For a tracking system containing M coils transmitting M distinct frequencies, the full generator magnetic model results in a $3 \times M$ matrix of magnetic flux densities given by

$$\mathbf{B}_{\text{FG}} = \left[\boldsymbol{B}_{\text{coil}_1}, \boldsymbol{B}_{\text{coil}_2}, \ldots, \boldsymbol{B}_{\text{coil}_\text{M}}\right] \tag{5}$$

where each $\boldsymbol{B}_{\text{coil}}$ is a vector of field components as shown in (3) due to a coil's total filament field as calculated in (4). In order to compactly define the coordinates of each coil, we define a $3 \times k$ coil definition matrix for each of the M coils in the field generator, $\mathbf{P}$, in (6). Fig. 4 illustrates a field generator containing $M = 8$ coils. Eight matrices are formed, $\mathbf{P}_1 \ldots \mathbf{P}_8$, where each $\mathbf{P}$ stores the consecutively ordered start and end points of the filaments for the respective coil. A row of ones is appended to allow manipulation of each matrix using homogeneous transformations

$$\mathbf{P} = \left[\boldsymbol{p}_1 \ \boldsymbol{p}_2 \ \cdots \ \boldsymbol{p}_k\right] = \begin{bmatrix} p_{x_1} & p_{x_2} & \cdots & p_{x_k} \\ p_{y_1} & p_{y_2} & \cdots & p_{x_k} \\ p_{z_1} & p_{z_2} & \cdots & p_{x_k} \\ 1 & 1 & \ldots & 1 \end{bmatrix}. \tag{6}$$

B. Multifield Generator Design

The shape and the monolithic design of the field generator coupled with the high manufacturing precision of the PCB process (10 µm) allow multiple generators to be treated identically. It is then possible to place multiple generators together and increase the overall system tracking volume. In this paper, we show results for two field generators, to create twice the effective volume of the single generator shown in Fig. 4.

We begin by introducing two identical field generators A and B as shown in Fig. 5. Generator B shares a common edge with A that is parallel to the y_A-axis and is inclined at an angle β. The Euclidean distance between the origin of both transmitters is given by $\boldsymbol{t}$. Combining this information allows

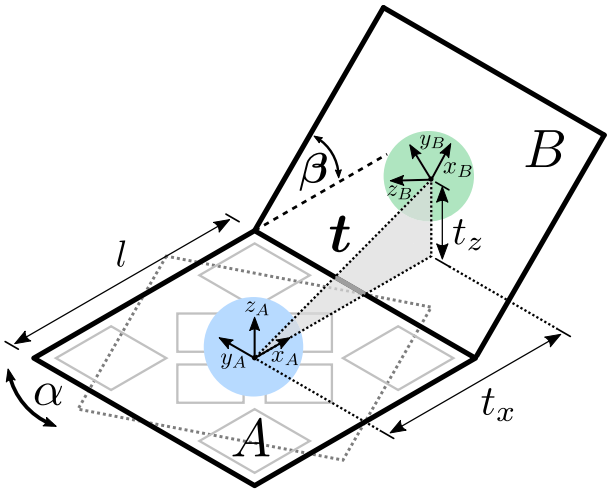

Fig. 5. Spatial relationship between two square field generators A and B. The planar generators are inclined at an angle β with respect to one another. If both generators touch at a common fulcrum, then the translation vector $\boldsymbol{t}$ pointing from the origin of generator A to that of generator B can be readily calculated from the transmitter length l.

for the creation of a single 4×4 homogeneous transformation matrix, which completely describes the location of generator B with respect to A given by

$$\mathbf{T}_B^A = \begin{bmatrix} \mathbf{R}_B^A & \mathbf{t}_B^A \\ \mathbf{0} & 1 \end{bmatrix} \tag{7}$$

where $\mathbf{R}_B^A$ describes the orientation of field generator B's frame with respect to A given by

$$\mathbf{R}_B^A = \mathbf{R}_y \mathbf{R}_z \tag{8}$$

where $\mathbf{R}_B^A$ is constructed using two elemental rotation matrices about the y- and z-axes of A, respectively, given by

$$\mathbf{R}_y = \begin{bmatrix} \cos(\beta) & 0 & \sin(\beta) \\ 0 & 1 & 0 \\ -\sin(\beta) & 0 & \cos(\beta) \end{bmatrix} \tag{9}$$

$$\mathbf{R}_z = \begin{bmatrix} \cos(\alpha) & -\sin(\alpha) & 0 \\ \sin(\alpha) & \cos(\alpha) & 0 \\ 0 & 0 & 1 \end{bmatrix}. \tag{10}$$

The translation vector $\mathbf{t}_B^A$ is defined as pointing from the origin of generator A to the origin of B given by

$$\mathbf{t}_B^A = \begin{bmatrix} t_x \\ t_y \\ t_z \end{bmatrix} = \begin{bmatrix} \frac{l}{2}(1 + \cos(\beta)) \\ 0 \\ l \sin(\beta) \end{bmatrix}. \tag{11}$$

The angle α that describes $\mathbf{R}_z$ is the initial rotation in the xy plane of generator B with respect to A. The angle β of $\mathbf{R}_y$ describes the inclination of B relative to A as shown in Fig. 5. If both field generators share a common edge as shown, then α is restricted to angles of 0°, 90°, 180°, and 270°. Angle β does not have this limitation and can be continuously varied while maintaining full contact along the common edge, although for experimental demonstration, we restrict ourselves to angles between 0° and 90°.

With this transform defined, the matrices defining the coil coordinates of generator B can be written in terms of those of A. Applying (7) to all coil matrices $\mathbf{P}_j$ of A yields the corresponding coil matrices of field generator B

$$\mathbf{P}_{jB} = \mathbf{T}_B^A \mathbf{P}_{jA} \tag{12}$$

where P_{jB} is the matrix of coordinates defining the position of each coil filament is shown in (6). This transformation allows the position of every coil to be defined in terms of the global reference frame of generator A. The total magnetic field at any point $\boldsymbol{r}$ relative to generator A can now be calculated for each coil using (2) and (4). This modeling technique can be readily scaled for multiple transmitters (*C, D,...*) providing an arbitrarily large tracking area. The primary constraint is that each field generator's location and orientation is referenced back to some global origin, which is defined as the reference frame of A in this case.

III. Field Generator Hardware

An open source EMT system [16], [19], [21] was used in this paper to obtain experimental results. A photograph of the system field generator and base station is shown in Fig. 6. The system field generator is fabricated on 1.6- mm PCB with 1-oz copper plating. Each generator board has two layers and contains eight identical coil windings aligned in a well-known configuration [22]. Each generator coil has an inductance of 70 μH and a resistance of 3 Ω. The specification for each coil winding is shown in Table I. The coil specification is used to procedurally generate the **P** matrices (6) for each coil in software.

The base station provides driving currents to each of the generator coils while also providing connectivity for up to 15 tracking sensors. Data acquisition is performed using an integrated USB-6212 OEM card (National Instruments, Austin, TX, USA). The card measures the induced voltage signal on the tracking sensors caused by the excitation current flowing in the field generators. A commercial 5-DoF tracking sensor (Model No. 610099, Northern Digital Inc, Waterloo, ON, Canada) was used for the experimental work. The generator current signal is also monitored in order to determine the phase angle between the transmitted magnetic field and the induced voltage signal. This angular information is used to resolve the axial orientation ambiguity associated with symmetric five degree-of-freedom magnetic sensors. Each base station is capable of driving an eight coil generator board. This paper uses two generators and, thus, requires two base stations to operate. The coils of each generator are excited by an ac signal at a unique frequency. Sixteen frequencies ranging from 18 to 33 kHz with 1- kHz spacing were chosen. The sensor position update rate was fixed at 30 Hz for all experiments in order to ensure deterministic time intervals between successive position measurements, although the system is capable of increased update speeds [21]. The connectivity between the base stations is illustrated in Fig. 7.

Fig. 8 shows the experimental setup for two generators labeled A and B. The origin of A is defined as the global reference frame. Generator B shares a common edge with A and is rotated by an angle α of 90° as indicated by the location of the cable connector. This orientation was chosen to minimize the mechanical warping of the circuit board due to the weight of the cable. Angle β can be adjusted to the desired value using the protractor. A precision machined polycarbonate test board with a thickness of 6 mm is used to mechanically locate the tracking sensor in known positions. The height of the test board is adjusted using Duplo bricks (The Lego Group, Billund, Denmark) with each brick measuring 19.2 mm in height with a manufacturing tolerance of 10 μm [23].

TABLE I
PCB Coil Specification

Property	*Value*
Seed length	70mm
Coil turns	25 turns
Track width	0.5mm
Track spacing	0.25mm
PCB Thickness	1.6mm

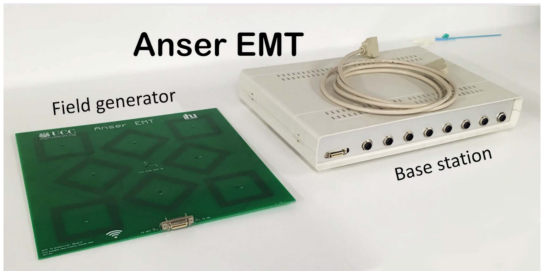

Fig. 6. Photograph of the EMT tracking system used for experimental work. The field generator comprises a PCB containing eight transmitter coils. Each coil transmits a unique frequency in the 10–30- kHz band as selected by the user. The base station provides signals for the transmitter and provides connectivity for up to 15 magnetic sensors.

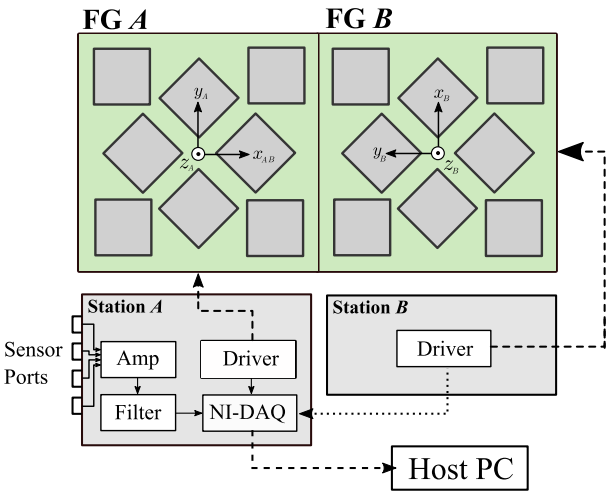

Fig. 7. Connectivity between the two base stations. Each station powers a single generator using an independent current driver circuit. Station A is used as the primary system for the tracking sensors. The DAQ of A is connected to the host PC and used for data acquisition. Station B is used solely as a current driver whose reference signal is fed back to the DAQ in station A.

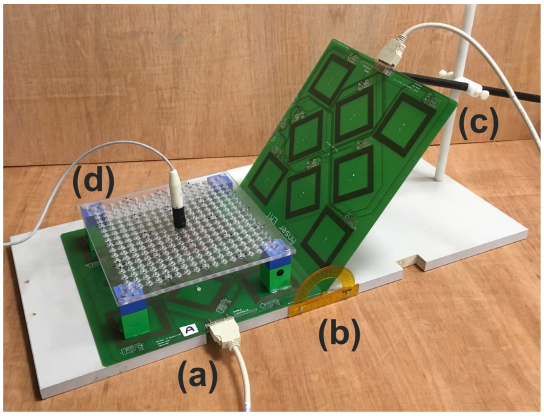

Fig. 8. Photograph of the experimental field generator setup. (a) Generator A is mounted with plastic screws onto a planar wooden frame. (b) Protractor is mounted to the wooden frame such that the fulcrum point is aligned with the edge of generator A. (c) Second generator B is mounted at an angle with respect to A using the protractor and an adjustable plastic rod. The configuration shown has $\alpha = 90°$ and $\beta = 45°$. (d) Precision machined polycarbonate test board is used in combination with Duplo to mechanically locate the test sensor at multiple locations above generator A.

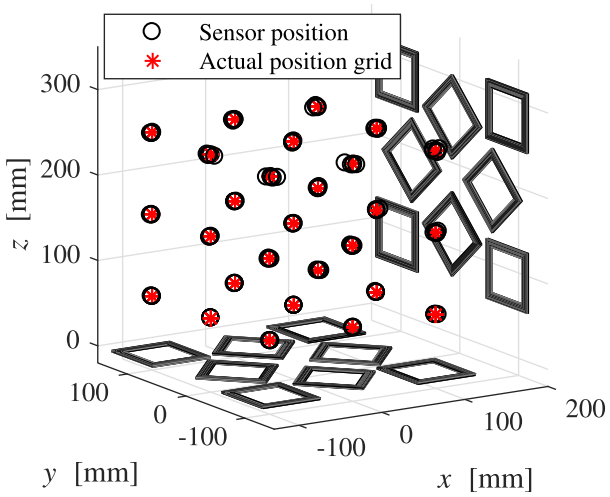

Fig. 9. Plot of grid points gathered for $\beta = 90°$. The generator coil filaments are also plotted for reference. Similar acquisitions were performed for angles $\beta = 0°$, 20°, 45°, and 70°.

IV. Experimental Methods

Two experiments were undertaken to validate the effectiveness of the multitransmitter design. The first experiment investigates the use of a second generator at a variable inclination angle on the overall precision and position accuracy of the system. The second experiment investigates the continuity performance of the system at the tracking volume boundary when both generators are horizontally tiled.

A. Angle Experiment

The introduction of field generator B provides additional magnetic fields whose spatial distribution is a function of the inclination angle β. Noncoplanar magnetic field generators, such as those used in orthogonal triaxial magnetic tracking systems, require only three generator coils to provide a sufficiently spatially unique magnetic field. Intuitively, the addition of generator B should increase the overall accuracy of the system. The setup shown in Fig. 8 was used with test grid heights of 66, 162, and 258 mm. Adopting a similar technique for the compact field generator design in [24], the tracking sensor was placed at nine equally spaced points on the test board's 3×3 point grid spaced 50 mm apart. 100 position measurements were acquired at each point. The acquisition is repeated for β angles of 0°, 20°, 45°, 70°, and 90°. A typical plot of the acquired position data for $\beta = 90°$ is shown in Fig. 9. A control measurement was also taken in which generator B was switched off and removed from the experimental setup.

Error measurements were determined by calculating the fiducial registration error (FRE) for each grid of nine points at $z = 66$, 162, and 258 mm. This method was adopted from [24] for testing the performance of a compact field generator tracking system in the absence of a ground-truth measurement. The calculation of the FRE begins by determining the rigid registration transformation, which best maps the acquired sensor position (*source*) points to the corresponding points in the test grid (*destination*) in a least-squares sense. This is performed using a well-known closed-form approach [25]. The FRE for a grid height z is then defined as the root-mean-square (rms) Euclidean distance between corresponding *source* and *destination* points after registration has been applied to the *source* points according to (13) [26]

$$\text{FRE} = \sqrt{\frac{1}{P}\sum_{i=1}^{P} |\mathbf{T}_R \boldsymbol{p}_{s_i} - \boldsymbol{p}_{d_i}|^2} \tag{13}$$

where $\boldsymbol{p}_{s_i}$ and $\boldsymbol{p}_{d_i}$ are corresponding *source* and *destination* points, respectively, $\mathbf{T}_R$ is the best fit rigid registration matrix between the two sets of points in a least-squared sense and $P = 9$.

The calculation of the precision (or jitter) is another important metric when evaluating magnetic tracking systems [27]. The precision at each grid position $\boldsymbol{r}$ was calculated as the rms error (RMSE) of the reported sensor position measurements with respect to the sample mean as follows:

$$\sigma_{\boldsymbol{r}} = \sqrt{\frac{1}{Q}\sum_{j=1}^{Q} |\boldsymbol{p}_{\boldsymbol{r}_j} - \bar{\boldsymbol{p}}_{\boldsymbol{r}}|^2} \tag{14}$$

where $\bar{\boldsymbol{p}}_{\boldsymbol{r}}$ is the sample mean over $Q = 100$ acquired position measurements at a single position within the grid. The jitter was calculated for heights of $z = 66$, 162, and 258 mm. The mean jitter for each grid height z was then calculated by taking the average of the nine individual jitter calculations.

B. Scribble Experiment

The simultaneous use of multiple field generators allows for the creation of larger tracking volumes. In certain circumstances, the common edge configuration shown in Fig. 5 may not be possible and a displacement may exist between the two transmitters. The experimental setup used to investigate the

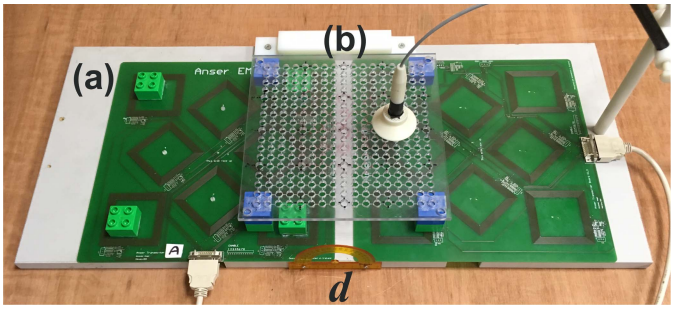

Fig. 10. Photograph of the experimental field generator setup for acquisition of planar points. (a) Generators A and B are placed in the same plane ($\beta = 0°$). (b) Machined test grid is placed in between both the generators. A 3-D-printed attachment allows the sensor to move smoothly on this plane. A displacement d exists between both the generators and is adjusted from 0 to 30 mm with the planar test grid recentered after each adjustment.

effect of this displacement is shown in Fig. 10. The tracking sensor was randomly scribbled in a single plane on the test grid at a fixed height of 66 mm. The test grid was centered on the gap d, which is varied between 0 and 30 mm in steps of 5 mm. 1000 random position measurements were acquired for each value of d. The error in z of each position measurement was calculated with respect to $d = 0$ measurement using the following equation:

$$\Delta z_k = z_k - \bar{z_0} \tag{15}$$

where z_k is the current position and $\bar{z_0}$ is the mean value of z when $d = 0$. The RMSE and the standard deviation of each point cloud were calculated from this data in the following equations, respectively,

$$\text{RMSE}_z = \sqrt{\frac{1}{Q}\sum_{k=1}^{Q}(\Delta z_k)^2} \tag{16}$$

$$\sigma_z = \sqrt{\frac{1}{Q}\sum_{k=1}^{Q}(\Delta z_k - \bar{\Delta z_k})^2} \tag{17}$$

where $\bar{\Delta z_k}$ is the mean z-coordinate over $Q = 1000$ position measurements of a particular point cloud.

V. Results

A. Error Versus Angle β Results

Figs. 11 and 12 summarize the accuracy and precision (jitter) of the system respectively at fixed heights of 66, 162, and 258 mm for different values of the inclination angle β. For heights of 66 and 162 mm above generator A, the FRE remains below 2 mm. The presence of generator B becomes significant at a heights of 258 mm above generator A. At this height, the control measurement exhibits the highest FRE of 10.6 mm, while the presence of an inclined generator B reduces the error to between 1.5 and 2.3 mm for angles between 45° and 90°. The observed trend shows that the FRE errors tend to reduce when generator B is inclined for large values of β, with the exception of $\beta = 90°$. Fig. 13 shows the frequency domain representation of the sampled sensor signal at a height of $z = 258$ mm for two angle configurations of generator B.

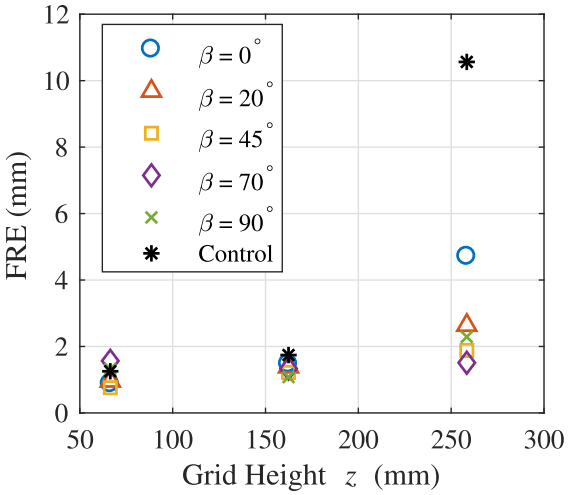

Fig. 11. FRE calculated using (13) for grid heights of 66, 162, and 258 mm above transmitter A for different angle configurations β of transmitter B. The control measurement with generator B powered off is also shown. The addition of transmitter B significantly reduces the grid registration error at large distances from the transmitter.

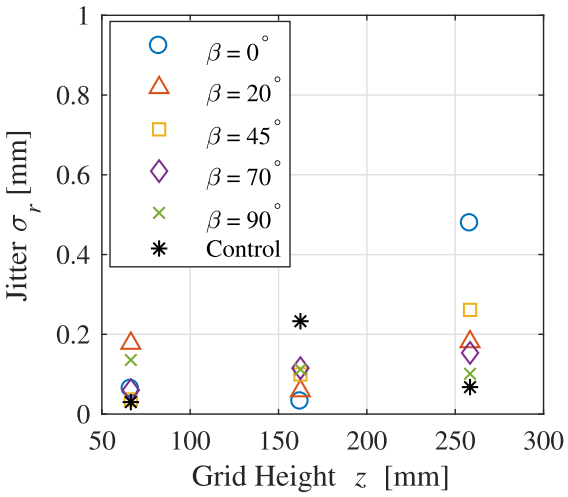

Fig. 12. RMS jitter error σ_r calculated using (14) for grid heights of 66, 162, and 258 mm above transmitter A for different angle configurations β of transmitter B. The control measurement with generator B powered off is also shown.

The signal-to-noise ratio (SNR) of the frequency components produced by generator B is improved for $\beta = 90°$, as the Euclidean distance between generator B and the sensor is reduced. SNR differences of up to 40 dB are observed between the two configurations.

B. Scribble Test Results

The scribble test results of Fig. 14 show how the separation between two field generators affects the overall system accuracy. A scatter plot of the results for $d = 0$, 15, and 30 mm is shown in Fig. 14. A bell-shape characteristic is observed for values of $d > 0$ mm, with the peak value of the bell increasing with d. The relationship between d and the rms error is plotted in Fig. 15.

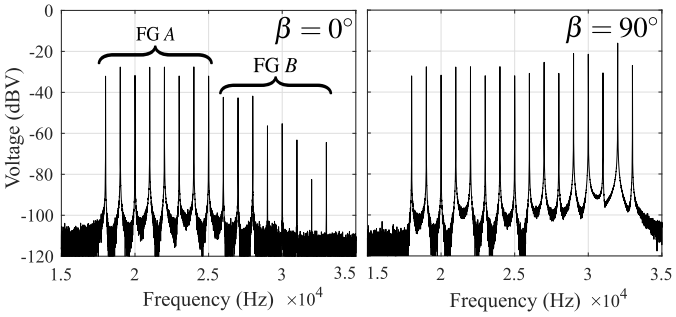

Fig. 13. Fast Fourier transform of the tracking sensor signal for $\beta = 0°$ and 90° after amplification. Each peak represents the induced voltage from a single generator coil. Spectra were acquired using 5000 sensor voltage samples with rectangular windowing. The sensor was located in the center of the test grid at $z = 258$ mm above generator A.

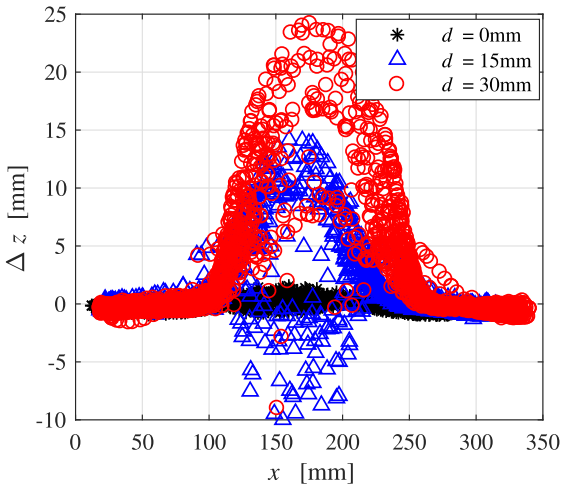

Fig. 14. Sensor error point cloud for transmitter separation distances of 0 mm (black), 15 mm (blue), and 30 mm (red). The 3-D coordinates are projected onto the xz plane for clarity and are referenced to the origin of generator A. The peaks of the point clouds shift in the positive x-direction due to the relative movement of generator B with respect to A; the peak error occurs at the center of the gap, $d/2$ mm from the edge of generator A.

VI. Discussion and Future Work

The results of Figs. 11 and 12 show that the addition of a secondary field generator increases the position tracking accuracy particularly at distances far from the primary field generator. The use of inclination angles between 45° and 90° seems to improve the accuracy of the tracking performance and decrease jitter above generator A. This correlates well with Fig 13, which shows that the sensor experiences an improved SNR at the fringes of the tracking volume when generator B is inclined at 90°.

The scribble tests identify the continuity performance of the tracking system when two field generators are placed side-by-side in the same plane. The results of Fig. 14 show that any gap $d > 0$ mm causes significant tracking error, where the maximum error occurs at the midpoint of the gap between the two field generators. The error characteristic is shown in Fig. 15 where it is clear that the error increases with larger gap sizes. We can conclude from this result that, for tiled field generators of this particular design, neighboring boards should

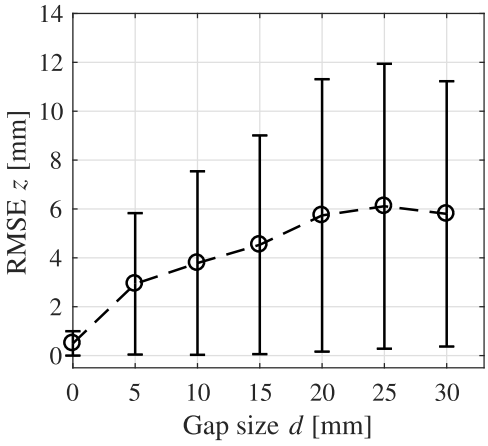

Fig. 15. RMS error of the z-coordinate data calculated using (16) plotted as a function of gap size d between 0 and 30 mm. Error bars indicate the standard deviation σ_z of each plot cloud's z-coordinates calculated using (17).

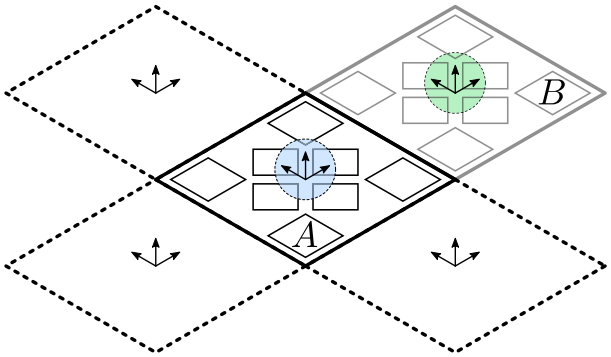

Fig. 16. Multiple planar field generators can be tiled to form larger tracking volumes. All transmitters share a common edge in order to preserve tracking continuity.

physically touch along a common edge in order to preserve tracking continuity.

This paper gathered results for two field generators. Expansion of this design for N field generators is possible allowing larger customizable tracking volumes can be constructed as shown in Fig. 16. Future work may study how to robustly implement a full tiling strategy while addressing limitations inherent in the current system design, such as transmission bandwidth and computational complexity. The system shown in this paper requires 16 unique frequencies with a uniform spacing of 1 kHz to achieve sufficient tracking performance. The requirement for all frequencies to be transmitted simultaneously (synchronous transmission) coupled with a system sampling rate of 100 kHz (i.e., Nyquist 50 kHz) results in bandwidth limitations occurring for $N > 6$ field generators since all constituent coils must have their own distinct transmission frequency. Increasing the system sampling rate alleviates the issue, but this will eventually be limited by some hardware-defined maximum. In this paper, the sampling rate limit is determined by the USB-6212 data acquisition unit (DAQ), which features a maximum sampling rate of 400 kHz. Scaling the system in this manner also increases the computational load on the host PC as the number of filaments in

the magnetic model scales linearly with the number of field generator coils as shown in (5). These constraints will need to be addressed when developing a full modular transmitter tiling strategy. Notwithstanding these limitations, this paper may represent a significant milestone in extending the volume of the accuracy of EMT technology, particularly in applications such as virtual reality and industrial robotics where system cost and modularity are beneficial.

VII. Conclusion

A novel method of creating custom magnetic tracking volumes has been demonstrated using PCB field generators. Positional accuracy improvements occur when an inclination angle exists between the field generators. Tiling of this particular design shows that errors are minimized when a common edge is shared between both the field generators. The system design may be easily scaled to create domain-specific tracking volumes which can be readily scaled for use in medical instrument tracking, robotics, and virtual reality applications.

References

[1] W. Kim, J. Song, and F. C. Park, "Closed-form position and orientation estimation for a three-axis electromagnetic tracking system," *IEEE Trans. Ind. Electron.*, vol. 65, no. 5, pp. 4331–4337, May 2018.

[2] A. M. Franz, T. Haidegger, W. Birkfellner, K. Cleary, T. M. Peters, and L. Maier-Hein, "Electromagnetic tracking in medicine—A review of technology, validation, and applications," *IEEE Trans. Med. Imag.*, vol. 33, no. 8, pp. 1702–1725, Aug. 2014.

[3] V. Pasku *et al.*, "A magnetic ranging-aided dead-reckoning positioning system for pedestrian applications," *IEEE Trans. Instrum. Meas.*, vol. 66, no. 5, pp. 953–963, May 2017.

[4] J. Včelák, P. Ripka, and A. Zikmund, "Long-range magnetic tracking system," *IEEE Sensors J.*, vol. 15, no. 1, pp. 491–496, Jan. 2015.

[5] A. Sheinker, B. Ginzburg, N. Salomonski, L. Frumkis, and B.-Z. Kaplan, "Localization in 3-D using beacons of low frequency magnetic field," *IEEE Trans. Instrum. Meas.*, vol. 62, no. 12, pp. 3194–3201, Dec. 2013.

[6] A. M. Franz *et al.*, "First clinical use of the echotrack guidance approach for radiofrequency ablation of thyroid gland nodules," *Int. J. Comput. Assist. Radiol. Surg.*, vol. 12, no. 6, pp. 931–940, Jun. 2017.

[7] H. A. Jaeger *et al.*, "Peripheral tumour targeting using open-source virtual bronchoscopy with electromagnetic tracking: A multi-user preclinical study," *Minimally Invasive Therapy Allied Technol.*, vol. 15, pp. 1–10, Nov. 2018.

[8] *NDI Tools and Sensors*. Accessed: Oct. 10, 2018. [Online]. Available: https://www.ndigital.com/medical/products/tools-and-sensors/

[9] A. Schwein *et al.*, "Electromagnetic tracking of flexible robotic catheters enables 'assisted navigation' and brings automation to endovascular navigation in an *in vitro* study," *J. Vascular Surg.*, vol. 67, no. 4, pp. 1274–1281, Apr. 2018.

[10] H. A. Jaeger *et al.*, "Automated catheter navigation with electromagnetic image guidance," *IEEE Trans. Biomed. Eng.*, vol. 64, no. 8, pp. 1972–1979, Aug. 2017.

[11] V. Pasku, A. de Angelis, G. de Angelis, A. Moschitta, and P. Carbone, "Magnetic field analysis for 3-D positioning applications," *IEEE Trans. Instrum. Meas.*, vol. 66, no. 5, pp. 935–943, May 2017.

[12] K. O'Donoghue and P. Cantillon-Murphy, "Low cost super-Nyquist asynchronous demodulation for use in em tracking systems," *IEEE Trans. Instrum. Meas.*, vol. 64, no. 2, pp. 458–466, Feb. 2015.

[13] A. Plotkin, O. Shafrir, E. Paperno, and D. M. Kaplan, "Magnetic eye tracking: A new approach employing a planar transmitter," *IEEE Trans. Biomed. Eng.*, vol. 57, no. 5, pp. 1209–1215, May 2010.

[14] H. Dai, S. Song, X. Zeng, S. Su, M. Lin, and M.-Q. Meng, "6-D electromagnetic tracking approach using uniaxial transmitting coil and tri-axial magneto-resistive sensor," *IEEE Sensors J.*, vol. 18, no. 3, pp. 1178–1186, Feb. 2018.

[15] W.-F. Loke, T.-Y. Choi, T. Maleki, L. Papiez, B. Ziaie, and B. Jung, "Magnetic tracking system for radiation therapy," *IEEE Trans. Biomed. Circuits Syst.*, vol. 4, no. 4, pp. 223–231, Aug. 2010.

[16] H. A. Jaeger *et al.*, "Anser EMT: The first open-source electromagnetic tracking platform for image-guided interventions," *Int. J. Comput. Assist. Radiol. Surg.*, vol. 12, no. 6, pp. 1059–1067, Jun. 2017.

[17] R. Byrd, R. Schnabel, and G. Shultz, "A trust region algorithm for nonlinearly constrained optimization," *SIAM J. Numer. Anal.*, vol. 24, no. 5, pp. 1152–1170, Oct. 1987.

[18] K. Levenberg, "A method for the solution of certain non-linear problems in least squares," *Quart. J. Appl. Math.*, vol. 2, no. 2, pp. 164–168, Jul. 1944.

[19] K. O'Donoghue *et al.*, "Catheter position tracking system using planar magnetics and closed loop current control," *IEEE Trans. Magn.*, vol. 50, no. 7, Jul. 2014, Art. no. 5100209.

[20] C. L. W. Sonntag, M. Sprée, E. A. Lomonova, J. L. Duarte, and A. J. A. Vandenput, "Accurate magnetic field intensity calculations for contactless energy transfer coils," in *Proc. 16th Int. Conf. Comput. Electromagn. Fields*, Aachen, Germany, Jun. 2007, pp. 25–28.

[21] H. A. Jaeger, S. Hinds, and P. Cantillon-Murphy, "An open framework enabling electromagnetic tracking in image-guided interventions," in *Proc. Int. Conf. Med. Image Comput. Comput.-Assist. Intervent. (MICCAI)*. Granada, Spain: Springer, Sep. 2018, pp. 168–175.

[22] A. Plotkin, E. Paperno, G. Vasserman, and R. Segev, "Magnetic tracking of eye motion in small, fast-moving animals," *IEEE Trans. Magn.*, vol. 44, no. 11, pp. 4492–4495, Nov. 2008.

[23] *Company Profile. An Introduction to the LEGO Group*, The LEGO Group, Billund, Denmark, 2010, p. 8.

[24] L. Maier-Hein *et al.*, "Standardized assessment of new electromagnetic field generators in an interventional radiology setting," *Med. Phys.*, vol. 39, no. 6, pp. 3424–3434, Jun. 2012.

[25] B. K. P. Horn, "Closed-form solution of absolute orientation using unit quaternions," *J. Opt. Soc. Amer. A*, vol. 4, no. 4, pp. 629–642, Apr. 1987.

[26] J. M. Fitzpatrick and J. B. West, "The distribution of target registration error in rigid-body point-based registration," *IEEE Trans. Med. Imag.*, vol. 20, no. 9, pp. 917–927, Sep. 2001.

[27] A. M. Franz *et al.*, "Standardized accuracy assessment of the calypso wireless transponder tracking system," *Phys. Med. Biol.*, vol. 59, no. 22, pp. 6797–6810, Nov. 2014.

Herman Alexander Jaeger (S'18–M'19) received the B.E., M.Eng.Sc., and Ph.D. degrees in electrical and electronic engineering from University College Cork (UCC), Cork, Ireland, in 2014, 2015, and 2018, respectively.

He is currently a Post-Doctoral Researcher with UCC. His current interests include electromagnetic tracking and navigation for image-guided interventions.

Pádraig Cantillon-Murphy (SM'18) received the B.E. degree in electrical and electronic engineering from University College Cork (UCC), Cork, Ireland, in 2003, and the M.S. and Ph.D. degrees from the Department of Electrical Engineering and Computer Science, Massachusetts Institute of Technology (MIT), Cambridge, MA, USA, in 2005 and 2008, respectively.

From 2008 to 2010, he was a Post-Doctoral Research Fellow with the Research Laboratory of Electronics, MIT. He was a Research Fellow with the Harvard Medical School, Brigham and Womens Hospital, Boston, MA, USA. He is currently a Lecturer of electrical and electronic engineering with UCC. His current research interests include magnetics in minimally invasive medical procedures and electromagnetic tracking.